HHS Public Access

Author manuscript

J Biomech. Author manuscript; available in PMC 2021 December 02.

Published in final edited form as:

J Biomech. 2020 December 02; 113: 110100. doi:10.1016/j.jbiomech.2020.110100.

Ex-vivo biomechanics of repaired rat intervertebral discs using genipin crosslinked fibrin adhesive hydrogel

Kengo Fujii[a,b], **Alon Lai**[a], **Nimrod Korda**[a], **Warren W. Hom**[a], **Thomas W. Evashwick-Rogler**[a,c], **Philip Nasser**[a], **Andrew C. Hecht**[a], **James C. Iatridis**[a,*]

[a]Leni & Peter W. May Department of Orthopaedics, Icahn School of Medicine at Mount Sinai, New York, NY, United States

[b]Department of Orthopaedic Surgery, University of Tsukuba, Tsukuba, Japan

[c]University of Pittsburgh School of Medicine, Pittsburgh, PA, United States

Abstract

Microdiscectomy is the current standard surgical treatment for intervertebral disc (IVD) herniation, however annulus fibrosus (AF) defects remain unrepaired which can alter IVD biomechanical properties and lead to reherniation, IVD degeneration and recurrent back pain. Genipin-crosslinked fibrin (FibGen) hydrogel is an injectable AF sealant previously shown to partially restore IVD motion segment biomechanical properties. A small animal model of herniation and repair is needed to evaluate repair potential for early-stage screening of IVD repair strategies prior to more costly large animal and eventual human studies. This study developed an *ex-vivo* rat caudal IVD herniation model and characterized torsional, axial tension–compression and stress relaxation biomechanical properties before and after herniation injury with or without repair using FibGen. Injury group involved an annular defect followed by removal of nucleus pulposus tissue to simulate a severe herniation while Repaired group involved FibGen injection. Injury significantly altered axial range of motion, neutral zone, torsional stiffness, torque range and stress-relaxation biomechanical parameters compared to Intact. FibGen repair restored the stress-relaxation parameters including effective hydraulic permeability indicating it effectively sealed the IVD defect, and there was a trend for improved tensile stiffness and axial neutral zone length. This study demonstrated a model for studying IVD herniation injury and repair strategies using rat caudal IVDs *ex-vivo* and demonstrated FibGen sealed IVDs to restore water retention and IVD pressurization. This *ex-vivo* small animal model may be modified for future *in-vivo* studies to screen IVD repair strategies using FibGen and other IVD repair biomaterials as an augment to additional large animal and human IVD testing.

Keywords

Intervertebral disc; Annulus fibrosus repair; Rat; Fibrin genipin; Biomechanics

*Corresponding author at: Leni & Peter W. May Department of Orthopaedics, Icahn School of Medicine at Mount Sinai, One Gustave Levy Place, Box 1188, New York, NY 10029 USA. James.iatridis@mssm.edu (J.C. Iatridis).

Conflict of interest statement

KF (None), AL (None), WWH (None), TER (None), PN (None), ACH (1 – Zimmer Spine; 3B – Zimmer, Medtronic), JCI (Unlicensed patent for FibGen for IVD repair).

1. Introduction

Microdiscectomy is the current standard surgical treatment for intervertebral disc (IVD) herniation, which is directly associated with radicular pain, and has an annual Medicare cost reported to be $300 million (Schoenfeld and Weiner, 2010). However, defects in the annulus fibrosus (AF) remain unrepaired following microdiscectomy, which can lead to re-herniation, accelerated degeneration and recurrent pain (Barth et al., 2008; McGirt et al., 2009b, 2009a). As a consequence, 5–21% of patients suffer from re-herniation following discectomy (Carragee et al., 2006). Poor innate IVD healing makes developing IVD repair biomaterials capable of sealing IVD defects and promoting repair a high priority (Buckley et al., 2018; Guterl et al., 2013).

Current repair strategies include nucleus pulposus (NP) repair, AF suture, AF closure devices, and injectable hydrogels (Bailey et al., 2013; Buckley et al., 2018; Chiang et al., 2011; Fujii et al., 2019; Guterl et al., 2013; Hom et al., 2019; Iatridis et al., 2013; Long et al., 2016b; Sloan et al., 2017, 2018, 2020; Virk et al., 2020). Suture of AF incisions did not significantly improve biomechanical properties of IVD following discectomy in sheep *in-vivo* (Ahlgren et al., 2000). The Barricaid AF closure device (Intrinsic Therapeutics, Woburn, MA) lowered the risk of symptomatic recurrence and reoperation (Kuršumović et al., 2020; Thomé et al., 2018; However, Barricaid requires vertebral anchoring with evidence for endplate damage, device subsidence, and no repair potential. Multiple biomaterial hydrogels are under development as AF repair strategies (Borem et al., 2019; Bowles and Setton, 2017; Bron et al., 2010; D'Este et al., 2018; Guillaume et al., 2014; Iatridis et al., 2013; Lin et al., 2019; Long et al., 2018; Pennicooke et al., 2018; Sloan et al., 2018). Structured biomaterials aim to emulate the native AF structure yet have limited integration with native tissue and face a relatively high risk for herniation and therefore have also been advanced for whole IVD replacement strategies (Gullbrand et al., 2018; Long et al., 2016b; Martin et al., 2015). AF repair patches are also in development to reduce this reherniation risk with mixed success (Borem et al., 2019; Long et al., 2016a). As these biomaterials are developed, they require screening to assess their capacity for sealing AF defects, restoring IVD biomechanical properties, and promoting healing, considered critical design goals of AF repair strategies (Iatridis et al., 2013).

Several injectable hydrogels for AF repair have been evaluated including alginate, agarose, gelatin, and collagen, as well as sponges made from polyglycolic acid (PGA), polylactic acid (PLA), poly(ε-caprolactone), collagen, silk, hyaluronic acid, and/or gly-cosaminoglycans, as reviewed by Bowles and Setton (Bowles and Setton, 2017). Injectable hydrogels offer appeal because they can be applied during discectomy or other minimally invasive procedures, fill void space and have been used with acellular and cellladen biomaterials (Bron et al., 2010; Lin et al., 2019; Panebianco et al., 2020; Sloan et al., 2020). Adhesive biomaterials can integrate with native IVD tissues in order to reduce herniation risk and can be tuned to emulate multiple material properties of the native AF or NP tissues yet as an injectable hydrogel, they do not succeed in matching tensile properties of the AF (Bowles and Setton, 2017; Bron et al., 2010; DiStefano et al., 2020; Grunert et al., 2014a; Lin et al., 2019; Panebianco et al., 2020). More recently, composite repair strategies have

been developed including both NP and AF repair, with one advancing to large animal in vivo studies (Hom et al., 2019; Sloan et al., 2020). In this study we investigate genipin-crosslinked fibrin (FibGen) hydrogel, which is an adhesive, void filling AF repair sealant (Likhitpanichkul et al., 2014). Fibrin is FDA approved for other indications and frequently used in surgery. Genipin is a plant-based chemical crosslinker that enhances stiffness and slows biomaterial resorption (Dare et al., 2009; Schek et al., 2011). FibGen can be tuned to match native AF shear properties, and can partially restore IVD motion segment biomechanical properties in a bovine *ex-vivo* model (Hom et al., 2019; Likhitpanichkul et al., 2014). One *in-vivo* study evaluated FibGen in an ovine cervical spine model and found FibGen integrated with surrounding AF tissue without herniation after one month and was resorbed after 12 months (Long et al., 2019). However, FibGen did not significantly improve repair compared to the injured control. Further *in-vivo* studies are necessary to track short-term healing and long-term repair to determine if FibGen can prevent IVD degeneration in a more severe injury model. FibGen has also been modified for cell delivery, requiring further evaluation (Cruz et al., 2018; Panebianco et al., 2020).

Models of large AF defects are required to assess the biomechanical and repair potential of FibGen and other IVD repair biomaterials. A systematic review showed high variability in the choice of AF repair models and selected output variables, making it difficult to compare across studies and demonstrating a need to develop standardized biomechanical models that can be repeatably applied across multiple laboratories in order to screen AF repair biomaterials and devices (Virk et al., 2020). Large animal models are often preferred due to the ability to apply high forces and greater similarity with the human spine in terms of size, structure, loading environment (Reitmaier et al., 2013; Smit, 2002), but are costly and consequently often involve relatively small sample sizes making their adaptation across many labs more difficult.

Small animal models are commonly used to study IVD degeneration and regeneration (Grunert et al., 2014b; Sloan et al., 2017; Sobajima et al., 2005; Boxberger et al., 2009; Singh et al., 2005), and to evaluate the biomaterials for IVD repair (Grunert et al., 2014a; Ishiguro et al., 2019; Martin et al., 2015, 2014; Takeoka et al., 2020). Rats are larger than mice facilitating surgical intervention and smaller and less costly than rabbits. Compared to lumbar IVDs, rat caudal IVDs have improved access for surgical interventions and are relatively larger, which improves the ability to more accurately induce injury, inject biomaterials, and prepare the specimens for biomechanical testing. Therefore, there is a need for an additional pre-clinical IVD repair screening model in small animals that would augment large animal and human studies. This study therefore developed an IVD herniation model in rat caudal IVDs with FibGen repair and biomechanical evaluation to determine whether small animal models may be used to screen repair strategies. A large IVD defect injury with AF injury and NP herniation was created to ensure sufficient space for biomaterial injection. This *ex-vivo* rat caudal IVD biomechanical study: 1) developed an IVD herniation model that was repaired with FibGen injection, and 2) determined whether FibGen could restore biomechanical properties to the intact conditions. We believe this important step demonstrates the possibility to use the rat model as a pre-clinical screening tool to evaluate the repair potential of FibGen and other IVD repair biomaterials in future small and large animals in vivo, and potentially human studies.

2. Methods

2.1. Study design

Skeletally mature Sprague Dawley male rat coccygeal motion segments (c4-5, c6-7 and c8-9) were isolated and randomly assigned into experimental groups: (1) Intact, (2) Injury, and (3) Repaired (n = 10/group) (Fig. 1A). Biomechanical properties of all specimens were initially tested intact. Specimens in Injury and Repaired groups were then injured to simulate microdiscectomy with the Injury group untreated and the Repaired group injected with FibGen. Specimens were biomechanically tested again. Intact group was tested twice with no injury or repair to identify the effects of two biomechanical tests. All samples were incubated at 37 °C in PBS for 3 h prior to the post-injury biomechanical measurement following similar procedures that ensure full FibGen polymerization (Cruz et al., 2017).

No live animals were used. All rat tails were obtained by tissue share from studies approved by Institutional Animal Care and Use Committee.

2.2. Preparation and potting of rat motion segment

Preparation and potting of rat motion segments were previously described (Lai et al., 2019; Mosley et al., 2019; Torre et al., 2019). Briefly, all surrounding tissues including vertebral processes were removed under a dissection microscope. Motion segments were dissected and stored in 1X phosphate-buffered saline (PBS) (Fisher Scientific, Hampton, NH) with protease inhibitor (complete cocktail tablet, Roche Diagnostics Corporation, Indianapolis, IN), at −20 °C until the day before testing. Motion segments were potted in two 10-mm custom stainless steel pots with an instant adhesive (Loctite 401, Henkel, Dusseldorf, Germany) and an accelerant (Loctite 712, Henkel, Dusseldorf, Germany). A custom clamp and plumb line confirmed motion segments were aligned along the axis of loading. Potted motion segments were submerged in 1X PBS with protease inhibitor, at 4 °C overnight to allow full hydration prior to testing. On the day of testing, the potted motion segments were thawed in 1X PBS at room temperature for 2 h.

2.3. IVD injury

After the pre-injury tests, potted specimens were fixed to a custom made compression-distraction tool attached to a digital caliper (Mitsutoyo, Kanagawa, Japan) to control compression-distraction distances. An 1 mm × 2 mm annular defect in the posterolateral region of IVDs was box cut by scalpel with removal of NP tissue in Injury and Repaired groups (Fig. 1A). NP tissue extrusion for removal by micro-forceps was achieved by compressing the IVD using the caliper system by 0.90 mm which repeatedly induced NP tissue herniation. This distance approaches the average rat tail disc height, although substantial deflection occurs in both vertebrae and IVDs during tail motion segments compression (MacLean et al., 2007; O'Connell et al., 2007).

2.4. Hydrogel preparation and injection

FibGen was prepared as previously described (Guterl et al., 2014; Hom et al., 2019). Briefly, 200 mg of bovine fibrinogen (Sigma-Aldrich, St. Louis, MO) was dissolved in 1140 μL of PBS and mixed with 40 U of thrombin (Sigma-Aldrich, St. Louis, MO) and 8 mg of genipin

(FUJIFILM Wako Chemicals U.S.A. Corporation, Richmond, VA) using a 4:1 dual barrel syringe, a mixing tip (Pac-Dent, Brea, CA) and a 10 μL micropipette tip. The process of intradiscal injection was performed with potted motion segment attached to the custom made compression-distraction tool and under dissecting microscope. The specimen was initially compressed to remove the air from injured IVD. The micropipette tip of the syringe was then placed into the injured IVD through the annular defect. FibGen was slowly injected into the IVD while the motion segment was slowly distracted back to its original height. This procedure generated a negative pressure which allowed the injected FibGen to fill up the intradiscal space without generating air bubbles during. FibGen was injected into the defect until a small amount of excess FibGen was injected outside the AF to ensure the IVD was entirely filled with FibGen, as might be expected in a surgical repair setting.

2.5. Biomechanical testing

Changes in motion segment biomechanical properties before and after annular injury with/without repair were measured using torsional, axial tension-compression, and stress relaxation tests (Fig. 1B) (Mosley et al., 2019; Torre et al., 2019). Firstly, torsional biomechanical testing was performed using an AR2000ex rheometer (TA instruments, New Castle, DE). An angular displacement-controlled cyclic testing protocol was used: samples were rotated to ±10° for 20 cycles at 1 Hz and the last complete cycle was used for data analyses. After torsional testing, motion segments were submerged in 1X PBS with protease inhibitor to rehydrate for 30 min.

Axial tension-compression biomechanical testing and stress relaxation testing were then performed using an Enduratec ELF 3200 (TA Instruments, New Castle, DE). Specimens were loaded cyclically in force control at ±0.5 MPa for 20 cycles at 0.5 Hz. Finally, stress relaxation tests were performed with ramp displacement applied until the force equivalent of 0.15 MPa compression was achieved, whereupon and the actuator was held at a constant position for 10 min.

All biomechanical testing was performed at room temperature.

2.6. Analysis of biomechanical testing

Biomechanical properties of torsional stiffness, torque range, compressive stiffness, tensile stiffness, range of motion (ROM), and torsional and axial neutral zone (NZ) length were determined from the torsional and axial tests (Fig. 2 & Fig. 3). Percent relaxation, time constant (τ) and effective hydraulic permeability were calculated from stress relaxation tests (Fig. 4) (Borde et al., 2015).

Custom MATLAB (Mathworks, Natrick, MA, USA) code was used to determine biomechanical parameters from torsional and axial data. Axial and torsional NZ length and stiffness were determined from the last complete test cycle as described (Di Pauli von Treuheim et al., 2020; Torre et al., 2019). Torsional stiffness values were defined as the slope of the top 20% of the loading portion of the torque-rotation curve then averaged from clockwise and counterclockwise rotation values. Torque range was the difference in peak values developed in ±10° rotation. NZ was calculated using the Stiffness Threshold method (Di Pauli von Treuheim et al., 2020). Compressive and tensile stiffness were calculated as

the slope of the linear upper 20% regions of the force-displacement curve. ROM was the total displacement from maximum compression to maximum tension. The axial displacement and slope of the NZ region were defined as the axial NZ length and NZ stiffness, respectively. Axial NZ length and stiffness were calculated using the Stiffness Threshold method (Di Pauli von Treuheim et al., 2020).

For stress relaxation testing, the stress vs time curve was fitted using a poroelastic model (Fig. 4B) as described (Borde et al., 2015). The relaxation time constant (τ), force constants (A & B), and the effective equilibrium modulus (E) were obtained from the curve fit, while the IVD radius (r) for all samples was taken as the average of posterior-anterior and lateral widths from previous study (Beckstein et al., 2008). The relaxation magnitude (%Relaxation) and the effective hydraulic permeability (k) of each IVD were calculated (Fig. 4B).

2.7. Radiographic measurement

IVD height was assessed using radiographs obtained prior to both pre-injury and post-injury biomechanical tests. Faxitron (Bioptics, LLC, Tucson, AZ) was used to obtain an anterior-posterior view radiograph image. Superior and inferior borders of the IVD were manually identified using ImageJ, and their coordinates were used to calculate the average distance between the borders using a custom MATLAB script. Disc height ratio was calculated as post-op disc height/pre-op disc height, as described (Evashwick-Rogler et al., 2018; Lai et al., 2019, 2016).

2.8. Statistical analysis

All post-injury data were normalized to their pre-injury values to eliminate variations between samples, and analyzed using Oneway ANOVA with Tukey's post-hoc tests. Statistical analyses were performed using Prism (GraphPad, San Diego, CA), and significance level $p < 0.05$.

3. Results

Torsional testing results showed significantly decreased torsional torque range, torsional stiffness following IVD injury as compared to Intact group ($p < 0.0001$) (Fig. 2) with relative and absolute values of all parameters and their statistical comparisons presented (Tables 1 and 2). None of the torsional parameters showed biomechanical restoration after repair. Axial tension-compression testing results showed significantly increased axial ROM and axial NZ length in injured IVDs when compared with intact IVDs ($p = 0.02$ for axial ROM and $p = 0.04$ for axial NZ length) (Fig. 3).

Decreased axial NZ length and tensile stiffness in Repaired group in comparison with Intact group suggests biomechanical restoration after IVD repair with FibGen, but there were no significant differences between Injured group and Repaired Group ($p = 0.77$ for NZ length and $p = 0.30$ for tensile stiffness, Injured group vs Repaired group).

Stress relaxation testing results showed significantly smaller % Relaxation in Injured group than in Intact group ($p = 0.03$), while there was no significant difference between Injured

and Repaired groups ($p = 0.38$) and Intact and Repaired groups ($p = 0.39$), which suggests that FibGen repair partially restores viscoelasticity of injured IVDs (Fig. 4). Furthermore, τ was lower in Injured group in both Intact and Repaired groups ($p = 0.0008$ for Intact vs Injured, $p = 0.002$ for Injured vs Repaired), while the effective hydraulic permeability was significantly higher in Injured group than in both Intact and Repaired groups ($p = 0.002$ for Intact vs Injured, $p = 0.005$ for Injured vs Repaired), which suggests that FibGen repair improves water retention within injured IVDs under stress.

No significant difference in disc height was observed between Intact, Injured and Repaired groups ($p = 0.15$) (Fig. 4).

4. Discussion

There is an unmet clinical need to develop IVD repair strategies capable of sealing IVD defects that remain unrepaired after herniation and discectomy procedures, and small animal models provide an additional early pre-clinical screening tool that can help accelerate translation. This study characterized biomechanical changes of rat caudal motion segments following discectomy and evaluated whether the changes could be restored by injectable FibGen hydrogel. The simulated discectomy injury significantly increased axial ROM, axial NZ length and hydraulic permeability, and significantly decreased torsional torque range, torsional stiffness, %relaxation and τ when compared to intact samples ($p < 0.05$; Figs. 2-4). IVD repair with intradiscal FibGen injection restored the altered viscoelasticity (i.e. %relaxation, $p > 0.05$ and τ, $p < 0.05$) and hydraulic permeability ($p < 0.05$) induced by IVD injury (Fig. 4) indicating that the hydrogel successfully sealed the large AF defects, and there was a trend for improved IVD height, tensile stiffness and axial NZ length.

Rat caudal IVDs have commonly been used to study IVD degeneration (Han et al., 2008; Hu et al., 2018; Iatridis et al., 1999; Lai et al., 2008; MacLean et al., 2003; Rousseau et al., 2007; Wuertz et al., 2009) and AF repair strategies (Borde et al., 2015; Grunert et al., 2014a; Kazezian et al., 2017; Nukaga et al., 2019). However, few rat studies (Sloan et al., 2017) have focused on modeling the large IVD defect that remains after discectomy. Caudal IVDs were chosen for this study since they are much more accessible than lumbar IVDs insofar as not requiring a transperitoneal or posterior percutaneous approach for injury, which makes caudal IVDs more advantageous for future *in-vivo* studies. In this study, we induced discectomy injury by making a box cut of 1 mm × 2 mm in AF followed by a compression to extrude NP tissue. This injury was relatively larger than previous studies inducing annular injury by stab or needle puncture (Beckstein et al., 2008; Elliott et al., 2008; Showalter et al., 2012; Torre et al., 2019). This larger injury was created to enable filling the defect with a viscous hydrogel, FibGen in this case. The box cut defect spanned >80% of the IVD height, although the decreased torque range and torsional stiffness measured in this study was similar to those from prior studies inducing the annular defect by needle puncture which spanned approximately 40% of the IVD height (Elliott et al., 2008; Torre et al., 2019). This suggests that the addition of NP removal did not have a significant impact on torsional parameters, which is not surprising since torsional testing is known to be most strongly affected by AF fiber integrity (Iatridis et al., 2013). Injury impacted axial NZ and ROM without significant changes in compressive or tensile stiffness, consistent with our previous

study (Torre et al., 2019). These observations differ from (Elliott et al., 2008) with decreased compression, tension and NZ stiffnesses, as well as increased NZ length. These differences may result from differences in test protocol. Overall, the discectomy injury in this study induced large and significant changes in viscoelasticity, hydraulic permeability, and several axial and torsional parameters and may serve as an additional pre-clinical tool to evaluate repair strategies.

FibGen has previously been evaluated using large animal injury models and shown promising results to integrate with surrounding AF tissue without herniation and partially restore IVD biomechanical properties (Likhitpanichkul et al., 2014; Long et al., 2016a; "Unable to find information for 6447834," n.d.). Further evaluation of FibGen is required to evaluate IVD healing, and refinements to enable delivery of cells and therapeutics in FibGen (Cruz et al., 2018; Hom et al., 2019; Long et al., 2019; Panebianco et al., 2020) also require screening. This rat discectomy model may be useful to allow biomechanical screening of biomaterials as a first step prior to *in-vivo* testing.

This study demonstrated FibGen could be directly injected into rat caudal IVDs following annular defect and NP removal. Injected FibGen was maintained in the IVDs following the mechanical tests. FibGen was able to partially restore %relaxation and fully restore τ and hydraulic permeability of the IVDs following injury, which indicated that the injected FibGen sealed the defects and restored IVD pressurization. The finding that the large AF injury had highly significant effects on viscoelastic behaviors (especially effective hydraulic permeability) that were restored with FibGen sealant, are very similar to the finding from Borde et al. that identified similar effects of the defect that were restored with collagen hydrogels (Borde et al., 2015). Together these 2 studies identify the high sensitivity of permeability to AF defects which result in loss of IVD pressurization. However, similar to results of our previous study using a large bovine caudal injury model (Hom et al., 2019), FibGen was unable to restore axial or torsional parameters back to intact levels. Importantly, the agreement between the large animal model and the current model suggests the rat IVD model may be useful in performing early studies to further investigate and optimize injectable hydrogels in a high-throughput manner. The lack of effect of FibGen on torsional parameters is not unexpected, since FibGen is an amorphous hydrogel that, while easily injectable, does not recapitulate the fiber structure of the native AF. Consequently, evaluations of healing with FibGen are particularly important and warrant further investigation. FibGen has demonstrated the ability to prevent IVD height loss in a previous long-term bovine organ culture study (Likhitpanichkul et al., 2014), and we believe these differences relate to differences in pre-loading condition prior to disc height measurements. However some of the lack of repair potential may be due to the relatively large defects created. Most importantly, FibGen restored stress relaxation parameters most effectively highlighting its capacity to seal IVD defects.

This study had some limitations. Operating on the small rat caudal IVDs was technically challenging and is a potential source of variance in Injured and Repaired samples. The use of our large injury was needed to enable direct injection of a highly viscous hydrogel into the small IVD space of the rat. This large size is a limitation since it would be relatively larger than injuries expected in large animal or herniated human IVDs, yet also provides greater

challenge to repair biomaterials. Some lack of biomechanical restoration from FibGen in this study as compared with prior studies in the literature (Likhitpanichkul et al., 2014; Long et al., 2016a) may be attributed to the relatively large defect in this study that might be near the limit of biomechanical improvements for FibGen, which suggests this model would not fully replicate the biomechanical conditions of injuries in large animal models and herniated human IVDs. We believe the large injury was justified since it enabled hydrogel repair within the IVD space of this small animal to offer another less expensive pre-clinical screening tool. Technically, generating negative pressure during the injection process was necessary to avoid the formation of air bubbles during the injection in this model. In large animal models or human trials, this technical problem would not be present provided FibGen is injected from the bottom of the defect. Following injection and biomechanical testing, selected samples were visually inspected under the dissecting microscope to confirm FibGen was still there and filled the void spaces. FibGen has adhesive strength of 20–70 kPa determined by pushout-testing which is similar to or greater than that of collagen gels (3–6 kPa) and a novel two part repair strategy involving dual modified glycosaminoglycan of with poly (ethylene glycol) diacrylate (8–15 kPa) determined by lap-shear testing (Cruz et al., 2017; DiStefano et al., 2020; Guterl et al., 2014; Jiang et al., 2019), yet adhesive strength values can vary with test protocol and other experimental conditions. Intact samples had some parameters with mean less than 1 when normalized (post/pre) suggesting that testing or storage could have some effects. While these reductions were not significantly reduced from 1, all experimental groups were similarly tested 2 times so any effects of testing protocol or storage conditions are not expected to affect relative comparisons between groups. To control for uniformity in the amount of NP tissue volume removed, we consistently compressed the same distance from the neutral condition using a digital caliper attached to the custom made pot clamp, thereby forcing a similar volume of NP tissue out of the annular defect for all samples. We considered a direct measurement of NP volume removed to be impossible to repeatedly perform accurately due to the ‘sticky’ and soft tissue and very small-volume of rat NP tissue.

We conclude that this herniation model of IVD injury and repair with *ex-vivo* rat caudal IVDs provides a model system to assess biomechanical performance and facilitates future pre-clinical *in-vivo* studies in a small animal IVD repair model. Intradiscal injection of FibGen successfully sealed IVD defects and partially restored multiple biomechanical properties altered with injury. Future *in-vivo* investigations are warranted for further evaluation of FibGen and other bioactive biomaterials for repair potential.

Acknowledgements

This work was supported by NIH/NIAMS Grants R01AR069315 & R01AR057397.

References

Ahlgren BD, Lui W, Herkowitz HN, Panjabi MM, Guiboux JP, 2000 Effect of anular repair on the healing strength of the intervertebral disc: a sheep model. Spine 25, 2165–2170. [PubMed: 10973397]

Bailey A, Araghi A, Blumenthal S, Huffmon GV, Anular Repair Clinical Study Group, 2013 Prospective, multicenter, randomized, controlled study of anular repair in lumbar discectomy: two-year follow-up. Spine 38, 1161–1169. [PubMed: 23392414]

Barth M, Weiss C, Thomé C, 2008 Two-year outcome after lumbar microdiscectomy versus microscopic sequestrectomy: part 1: evaluation of clinical outcome. Spine 33, 265–272. [PubMed: 18303458]

Beckstein JC, Sen S, Schaer TP, Vresilovic EJ, Elliott DM, 2008 Comparison of animal discs used in disc research to human lumbar disc. Spine 33, E166–E173. [PubMed: 18344845]

Borde B, Grunert P, Härtl R, Bonassar LJ, 2015 Injectable, high-density collagen gels for annulus fibrosus repair: an in vitro rat tail model. J. Biomed. Mater. Res. A 103, 2571–2581. [PubMed: 25504661]

Borem R, Madeline A, Vela R, Gill S, Mercuri J, 2019 Multi-laminate annulus fibrosus repair scaffold with an interlamellar matrix enhances impact resistance, prevents herniation and assists in restoring spinal kinematics. J. Mech. Behav. Biomed. Mater 95, 41–52. [PubMed: 30953808]

Bowles RD, Setton LA, 2017 Biomaterials for intervertebral disc regeneration and repair. Biomaterials 129, 54–67. [PubMed: 28324865]

Bron JL, van der Veen AJ, Helder MN, van Royen BJ, Smit TH, Skeletal Tissue Engineering Group Amsterdam, Research Institute MOVE, 2010 Biomechanical and in vivo evaluation of experimental closure devices of the annulus fibrosus designed for a goat nucleus replacement model. Eur. Spine J 19, 1347–1355. [PubMed: 20401620]

Boxberger JI et al., 2009 An in vivo model of reduced nucleus pulposus glycosaminoglycan content in the rat lumbar intervertebral disc. Spine 33 (2), 146–154. 10.1097/BRS.0b013e31816054f8.

Buckley CT, Hoyland JA, Fujii K, Pandit A, Iatridis JC, Grad S, 2018 Critical aspects and challenges for intervertebral disc repair and regeneration-Harnessing advances in tissue engineering. JOR Spine 1, e1029. [PubMed: 30895276]

Carragee EJ, Spinnickie AO, Alamin TF, Paragioudakis S, 2006 A prospective controlled study of limited versus subtotal posterior discectomy: short-term outcomes in patients with herniated lumbar intervertebral discs and large posterior anular defect. Spine 31, 653–657. [PubMed: 16540869]

Chiang C-J, Cheng C-K, Sun J-S, Liao C-J, Wang Y-H, Tsuang Y-H, 2011 The effect of a new anular repair after discectomy in intervertebral disc degeneration: an experimental study using a porcine spine model. Spine 36, 761–769. [PubMed: 20683387]

Cruz MA, Hom WW, DiStefano TJ, Merrill R, Torre OM, Lin HA, Hecht AC, Illien-Junger S, Iatridis JC, 2018 Cell-seeded adhesive biomaterial for repair of annulus fibrosus defects in intervertebral discs. Tissue Eng. Part A 24, 187–198. [PubMed: 29214889]

Cruz MA, McAnany S, Gupta N, Long RG, Nasser P, Eglin D, Hecht AC, Illien-Junger S, Iatridis JC, 2017 Structural and chemical modification to improve adhesive and material properties of fibrin-genipin for repair of annulus fibrosus defects in intervertebral disks. J. Biomech. Eng 139.

D'Este M, Eglin D, Alini M, 2018 Lessons to be learned and future directions for intervertebral disc biomaterials. Acta Biomater. 78, 13–22. [PubMed: 30092378]

Dare EV, Griffith M, Poitras P, Kaupp JA, Waldman SD, Carlsson DJ, Dervin G, Mayoux C, Hincke MT, 2009 Genipin cross-linked fibrin hydrogels for in vitro human articular cartilage tissue-engineered regeneration. Cells Tissues Organs (Print) 190, 313–325.

DiStefano TJ, Shmukler JO, Danias G, Pauli D.i., von Treuheim T, Hom WW, Goldberg DA, Laudier DM, Nasser PR, Hecht AC, Nicoll SB, Iatridis JC, 2020 Development of a two-part biomaterial adhesive strategy for annulus fibrosus repair and ex vivo evaluation of implant herniation risk. Biomaterials 258, 120309. [PubMed: 32823020]

Di Pauli von Treuheim T, Torre OM, Mosley GE, Nasser P, Iatridis JC, 2020 Measuring the neutral zone of spinal motion segments: comparison of multiple analysis methods to quantify spinal instability. JOR Spine 3, e1088. [PubMed: 32613163]

Elliott DM, Yerramalli CS, Beckstein JC, Boxberger JI, Johannessen W, Vresilovic EJ, 2008 The effect of relative needle diameter in puncture and sham injection animal models of degeneration. Spine 33, 588–596. [PubMed: 18344851]

Evashwick-Rogler TW, Lai A, Watanabe H, Salandra JM, Winkelstein BA, Cho SK, Hecht AC, Iatridis JC, 2018 Inhibiting tumor necrosis factor-alpha at time of induced intervertebral disc injury limits long-term pain and degeneration in a rat model. JOR Spine 1.

Fujii K, Yamazaki M, Kang JD, Risbud MV, Cho SK, Qureshi SA, Hecht AC, Iatridis JC, 2019 Discogenic back pain: literature review of definition, diagnosis, and treatment. JBMR PLUS 3, e10180. [PubMed: 31131347]

Grunert P, Borde BH, Hudson KD, Macielak MR, Bonassar LJ, Härtl R, 2014a Annular repair using high-density collagen gel: a rat-tail in vivo model. Spine 39, 198–206. [PubMed: 24253790]

Grunert P, Gebhard HH, Bowles RD, James AR, Potter HG, Macielak M, Hudson KD, Alimi M, Ballon DJ, Aronowitz E, Tsiouris AJ, Bonassar LJ, Härtl R, 2014b Tissue-engineered intervertebral discs: MRI results and histology in the rodent spine. J. Neurosurg. Spine 20, 443–451. [PubMed: 24527831]

Guillaume O, Daly A, Lennon K, Gansau J, Buckley SF, Buckley CT, 2014 Shape-memory porous alginate scaffolds for regeneration of the annulus fibrosus: effect of TGF-β3 supplementation and oxygen culture conditions. Acta Biomater. 10, 1985–1995. [PubMed: 24380722]

Gullbrand SE, Ashinsky BG, Bonnevie ED, Kim DH, Engiles JB, Smith LJ, Elliott DM, Schaer TP, Smith HE, Mauck RL, 2018 Long-term mechanical function and integration of an implanted tissue-engineered intervertebral disc. Sci. Transl. Med 10.

Guterl CC, See EY, Blanquer SBG, Pandit A, Ferguson SJ, Benneker LM, Grijpma DW, Sakai D, Eglin D, Alini M, Iatridis JC, Grad S, 2013 Challenges and strategies in the repair of ruptured annulus fibrosus. Eur. Cell. Mater 25, 1–21. [PubMed: 23283636]

Guterl CC, Torre OM, Purmessur D, Dave K, Likhitpanichkul M, Hecht AC, Nicoll SB, Iatridis JC, 2014 Characterization of mechanics and cytocompatibility of fibrin-genipin annulus fibrosus sealant with the addition of cell adhesion molecules. Tissue Eng. Part A 20, 2536–2545. [PubMed: 24684314]

Han B, Zhu K, Li F-C, Xiao Y-X, Feng J, Shi Z-L, Lin M, Wang J, Chen Q-X, 2008 A simple disc degeneration model induced by percutaneous needle puncture in the rat tail. Spine 33, 1925–1934. [PubMed: 18708924]

Hom WW, Tschopp M, Lin HA, Nasser P, Laudier DM, Hecht AC, Nicoll SB, Iatridis JC, 2019 Composite biomaterial repair strategy to restore biomechanical function and reduce herniation risk in an ex vivo large animal model of intervertebral disc herniation with varying injury severity. PLoS ONE 14, e0217357. [PubMed: 31136604]

Hu M-H, Yang K-C, Chen Y-J, Sun Y-H, Lin F-H, Yang S-H, 2018 Optimization of puncture injury to rat caudal disc for mimicking early degeneration of intervertebral disc. J. Orthop. Res 36, 202–211. [PubMed: 28594131]

Iatridis JC, Mente PL, Stokes IA, Aronsson DD, Alini M, 1999 Compression-induced changes in intervertebral disc properties in a rat tail model. Spine 24, 996–1002. [PubMed: 10332792]

Iatridis JC, Nicoll SB, Michalek AJ, Walter BA, Gupta MS, 2013 Role of biomechanics in intervertebral disc degeneration and regenerative therapies: what needs repairing in the disc and what are promising biomaterials for its repair?. Spine J. 13, 243–262. [PubMed: 23369494]

Ishiguro H, Kaito T, Yarimitsu S, Hashimoto K, Okada R, Kushioka J, Chijimatsu R, Takenaka S, Makino T, Sakai Y, Moriguchi Y, Otsuru S, Hart DA, Fujie H, Nakamura N, Yoshikawa H, 2019 Intervertebral disc regeneration with an adipose mesenchymal stem cell-derived tissueengineered construct in a rat nucleotomy model. Acta Biomater. 87, 118–129. [PubMed: 30690206]

Jiang EY, Sloan SR, Wipplinger C, Kirnaz S, Härtl R, Bonassar LJ, 2019 Proteoglycan removal by chondroitinase ABC improves injectable collagen gel adhesion to annulus fibrosus. Acta Biomater. 97, 428–436. [PubMed: 31425894]

Kazezian Z, Sakai D, Pandit A, 2017 Hyaluronic acid microgels modulate inflammation and key matrix molecules toward a regenerative signature in the injured annulus fibrosus. Adv. Biosys 1.

Kuršumović A, Bouma GJ, Miller LE, Assaker R, Van de Kelft E, Hes R, Kienzler JC, 2020 Clinical implications of vertebral endplate disruptions after lumbar discectomy: 3-year results from a randomized trial of a bone-anchored annular closure device. J. Pain Res 13, 669–675. [PubMed: 32280269]

Lai A, Chow DHK, Siu SW, Leung SS, Lau EFL, Tang FH, Pope MH, 2008 Effects of static compression with different loading magnitudes and durations on the intervertebral disc: an in vivo rat-tail study. Spine 33, 2721–2727. [PubMed: 19050577]

Lai A, Ho L, Evashwick-Rogler TW, Watanabe H, Salandra J, Winkelstein BA, Laudier D, Hecht AC, Pasinetti GM, Iatridis JC, 2019 Dietary polyphenols as a safe and novel intervention for modulating pain associated with intervertebral disc degeneration in an in-vivo rat model. PLoS ONE 14, e0223435. [PubMed: 31577822]

Lai A, Moon A, Purmessur D, Skovrlj B, Laudier DM, Winkelstein BA, Cho SK, Hecht AC, Iatridis JC, 2016 Annular puncture with tumor necrosis factoralpha injection enhances painful behavior with disc degeneration in vivo. Spine J. 16, 420–431. [PubMed: 26610672]

Likhitpanichkul M, Dreischarf M, Illien-Junger S, Walter BA, Nukaga T, Long RG, Sakai D, Hecht AC, Iatridis JC, 2014 Fibrin-genipin adhesive hydrogel for annulus fibrosus repair: performance evaluation with large animal organ culture, in situ biomechanics, and in vivo degradation tests. Eur. Cell. Mater 28, 25–37. discussion 37. [PubMed: 25036053]

Lin HA, Varma DM, Hom WW, Cruz MA, Nasser PR, Phelps RG, Iatridis JC, Nicoll SB, 2019 Injectable cellulose-based hydrogels as nucleus pulposus replacements: assessment of in vitro structural stability, ex vivo herniation risk, and in vivo biocompatibility. J. Mech. Behav. Biomed. Mater 96, 204–213. [PubMed: 31054515]

Long RG, Bürki A, Zysset P, Eglin D, Grijpma DW, Blanquer SBG, Hecht AC, Iatridis JC, 2016a Mechanical restoration and failure analyses of a hydrogel and scaffold composite strategy for annulus fibrosus repair. Acta Biomater. 30, 116–125. [PubMed: 26577987]

Long RG, Ferguson SJ, Benneker LM, Sakai D, Li Z, Pandit A, Grijpma DW, Eglin D, Zeiter S, Schmid T, Eberli U, Nehrbass D, Di Pauli von Treuheim T, Alini M, Iatridis JC, Grad S, 2019 Morphological and biomechanical effects of annulus fibrosus injury and repair in an ovine cervical model. JOR Spine.

Long RG, Rotman SG, Hom WW, Assael DJ, Illien-Jünger S, Grijpma DW, Iatridis JC, 2018 In vitro and biomechanical screening of polyethylene glycol and poly(trimethylene carbonate) block copolymers for annulus fibrosus repair. J. Tissue Eng. Regen. Med 12, e727–e736. [PubMed: 27860368]

Long RG, Torre OM, Hom WW, Assael DJ, Iatridis JC, 2016b Design requirements for annulus fibrosus repair: review of forces, displacements, and material properties of the intervertebral disk and a summary of candidate hydrogels for repair. J. Biomech. Eng 138, 021007. [PubMed: 26720265]

MacLean JJ, Lee CR, Grad S, Ito K, Alini M, Iatridis JC, 2003 Effects of immobilization and dynamic compression on intervertebral disc cell gene expression in vivo. Spine 28, 973–981. [PubMed: 12768134]

MacLean JJ, Owen JP, Iatridis JC, 2007 Role of endplates in contributing to compression behaviors of motion segments and intervertebral discs. J. Biomech 40, 55–63. [PubMed: 16427060]

Martin JT, Milby AH, Chiaro JA, Kim DH, Hebela NM, Smith LJ, Elliott DM, Mauck RL, 2014 Translation of an engineered nanofibrous disc-like angle-ply structure for intervertebral disc replacement in a small animal model. Acta Biomater. 10, 2473–2481. [PubMed: 24560621]

Martin JT, Milby AH, Ikuta K, Poudel S, Pfeifer CG, Elliott DM, Smith HE, Mauck RL, 2015 A radiopaque electrospun scaffold for engineering fibrous musculoskeletal tissues: scaffold characterization and in vivo applications. Acta Biomater. 26, 97–104. [PubMed: 26248165]

McGirt MJ, Ambrossi GLG, Datoo G, Sciubba DM, Witham TF, Wolinsky J-P, Gokaslan ZL, Bydon A, 2009a Recurrent disc herniation and long-term back pain after primary lumbar discectomy: review of outcomes reported for limited versus aggressive disc removal. Neurosurgery 64, 338–344. discussion 344. [PubMed: 19190461]

McGirt MJ, Eustacchio S, Varga P, Vilendecic M, Trummer M, Gorensek M, Ledic D, Carragee EJ, 2009b A prospective cohort study of close interval computed tomography and magnetic resonance imaging after primary lumbar discectomy: factors associated with recurrent disc herniation and disc height loss. Spine 34, 2044–2051. [PubMed: 19730212]

Mosley GE, Hoy RC, Nasser P, Kaseta T, Lai A, Evashwick-Rogler TW, Lee M, Iatridis JC, 2019 Sex differences in rat intervertebral disc structure and function following annular puncture injury. Spine 44, 1257–1269. [PubMed: 30973506]

Nukaga T, Sakai D, Schol J, Sato M, Watanabe M, 2019 Annulus fibrosus cell sheets limit disc degeneration in a rat annulus fibrosus injury model. JOR Spine 2, e1050. [PubMed: 31463464]

O'Connell GD, Vresilovic EJ, Elliott DM, 2007 Comparison of animals used in disc research to human lumbar disc geometry. Spine 32, 328–333. [PubMed: 17268264]

Panebianco CJ, DiStefano TJ, Mui B, Hom WW, Iatridis JC, 2020 Crosslinker concentration controls TGFβ-3 release and annulus fibrosus cell apoptosis in genipin-crosslinked fibrin hydrogels. eCM 39, 211–226. [PubMed: 32396210]

Pennicooke B, Hussain I, Berlin C, Sloan SR, Borde B, Moriguchi Y, Lang G, Navarro-Ramirez R, Cheetham J, Bonassar LJ, Härtl R, 2018 Annulus fibrosus repair using high-density collagen gel: an in vivo ovine model. Spine 43, E208–E215. [PubMed: 28719551]

Reitmaier S, Schmidt H, Ihler R, Kocak T, Graf N, Ignatius A, Wilke H-J, 2013 Preliminary investigations on intradiscal pressures during daily activities: an in vivo study using the merino sheep. PLoS ONE 8, e69610. [PubMed: 23894509]

Rousseau M-A-A, Ulrich JA, Bass EC, Rodriguez AG, Liu JJ, Lotz JC, 2007 Stab incision for inducing intervertebral disc degeneration in the rat. Spine 32, 17–24. [PubMed: 17202887]

Schek RM, Michalek AJ, Iatridis JC, 2011 Genipin-crosslinked fibrin hydrogels as a potential adhesive to augment intervertebral disc annulus repair. Eur. Cell. Mater 21, 373–383. [PubMed: 21503869]

Schoenfeld AJ, Weiner BK, 2010 Treatment of lumbar disc herniation: evidencebased practice. Int. J. Gen. Med 3, 209–214. [PubMed: 20689695]

Showalter BL, Beckstein JC, Martin JT, Beattie EE, Espinoza Orías AA, Schaer TP, Vresilovic EJ, Elliott DM, 2012 Comparison of animal discs used in disc research to human lumbar disc: torsion mechanics and collagen content. Spine 37, E900–7. [PubMed: 22333953]

Singh K et al., 2005 Animal models for human disc degeneration. Spine J. 5 (6 Suppl), 267S–279S. 10.1016/j.spinee.2005.02.016. [PubMed: 16291123]

Sloan SR, Galesso D, Secchieri C, Berlin C, Hartl R, Bonassar LJ, 2017 Initial investigation of individual and combined annulus fibrosus and nucleus pulposus repair ex vivo. Acta Biomater. 59, 192–199. [PubMed: 28669721]

Sloan SR, Lintz M, Hussain I, Hartl R, Bonassar LJ, 2018 Biologic annulus fibrosus repair: a review of preclinical in vivo investigations. Tissue Eng. Part B Rev 24, 179–190 [PubMed: 29105592]

Sloan SR, Wipplinger C, Kirnaz S, Navarro-Ramirez R, Schmidt F, McCloskey D, Pannellini T, Schiavinato A, Härtl R, Bonassar LJ, 2020 Combined nucleus pulposus augmentation and annulus fibrosus repair prevents acute intervertebral disc degeneration after discectomy. Sci. Transl. Med 12.

Smit TH, 2002 The use of a quadruped as an in vivo model for the study of the spine - biomechanical considerations. Eur. Spine J 11, 137–144. [PubMed: 11956920]

Sobajima S, Kompel JF, Kim JS, Wallach CJ, Robertson DD, Vogt MT, Kang JD, Gilbertson LG, 2005 A slowly progressive and reproducible animal model of intervertebral disc degeneration characterized by MRI, X-ray, and histology. Spine 30, 15–24. [PubMed: 15626975]

Takeoka Y, Yurube T, Morimoto K, Kunii S, Kanda Y, Tsujimoto R, Kawakami Y, Fukase N, Takemori T, Omae K, Kakiuchi Y, Miyazaki S, Kakutani K, Takada T, Nishida K, Fukushima M, Kuroda R, 2020 Reduced nucleotomyinduced intervertebral disc disruption through spontaneous spheroid formation by the Low Adhesive Scaffold Collagen (LASCol). Biomaterials 235, 119781. [PubMed: 31981764]

Thomé C, Klassen PD, Bouma GJ, Kuršumović A, Fandino J, Barth M, Arts M, van den Brink W, Bostelmann R, Hegewald A, Heidecke V, Vajkoczy P, Fröhlich S, Wolfs J, Assaker R, Van de Kelft E, Köhler H-P, Jadik S, Eustacchio S, Hes R, Annular Closure RCT Study Group, 2018 Annular closure in lumbar microdiscectomy for prevention of reherniation: a randomized clinical trial. Spine J. 18, 2278–2287. [PubMed: 29730458]

Torre OM, Evashwick-Rogler TW, Nasser P, Iatridis JC, 2019 Biomechanical test protocols to detect minor injury effects in intervertebral discs. J. Mech. Behav. Biomed. Mater 95, 13–20. [PubMed: 30947120]

Virk S, Chen T, Meyers KN, Lafage V, Schwab F, Maher SA, 2020 Comparison of biomechanical studies of disc repair devices based on a systematic review. Spine J. 20, 1344–1355. [PubMed: 32092506]

Wuertz K, Godburn K, MacLean JJ, Barbir A, Donnelly JS, Roughley PJ, Alini M, Iatridis JC, 2009 In vivo remodeling of intervertebral discs in response to short- and long-term dynamic compression. J. Orthop. Res 27, 1235–1242. [PubMed: 19274755]

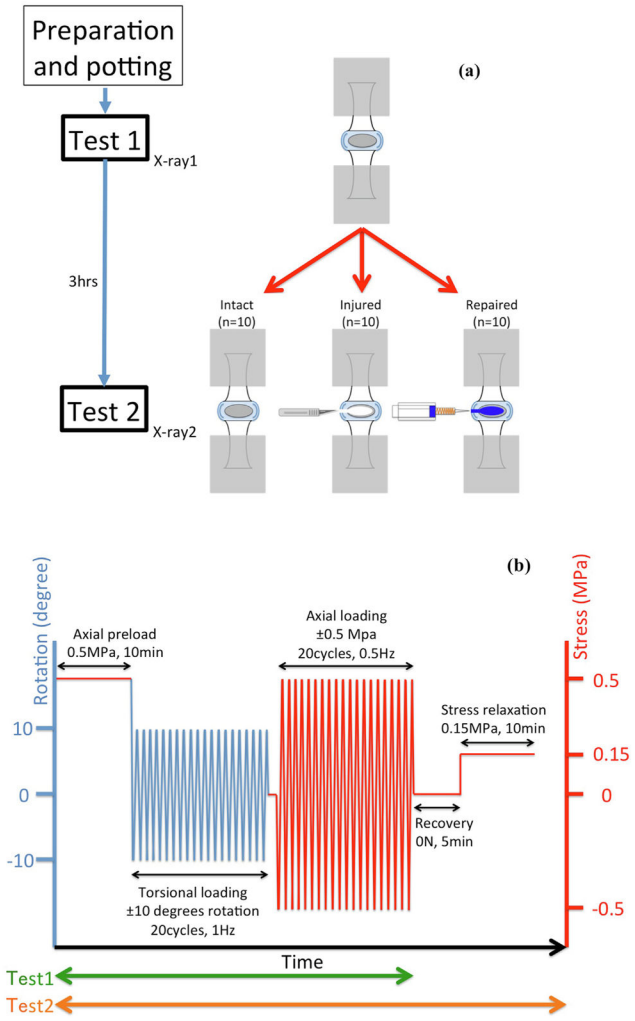

Fig. 1.

Schematic of study design, experimental groups, and biomechanical testing protocol. (A) Schematic of experimental groups, injury, repair and repeated tests. (B) Loading protocol used for torsional and axial cyclic mechanical testing, and stress relaxation test.

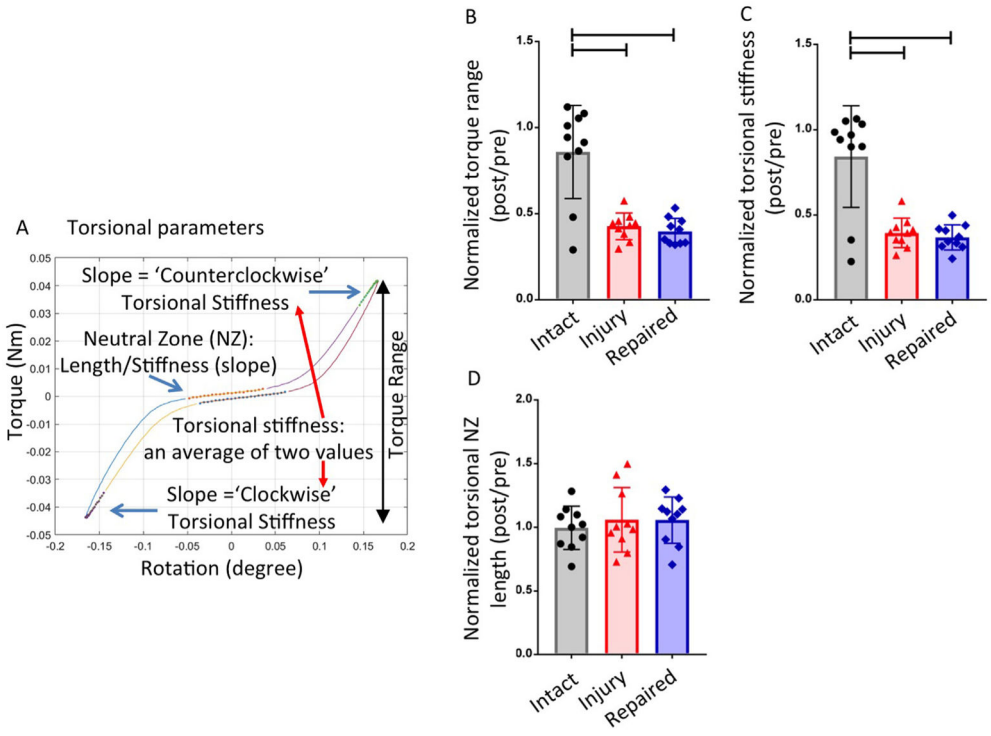

Fig. 2.

Torsional testing results. (A) Representative torque-rotation curve which shows the regions of the curve analyzed to calculate torsional parameters. (B) Results of Torque range (C) Results of torsional stiffness (D) Results of torsional neutral zone (NZ) length. Bar indicates $p < 0.05$.

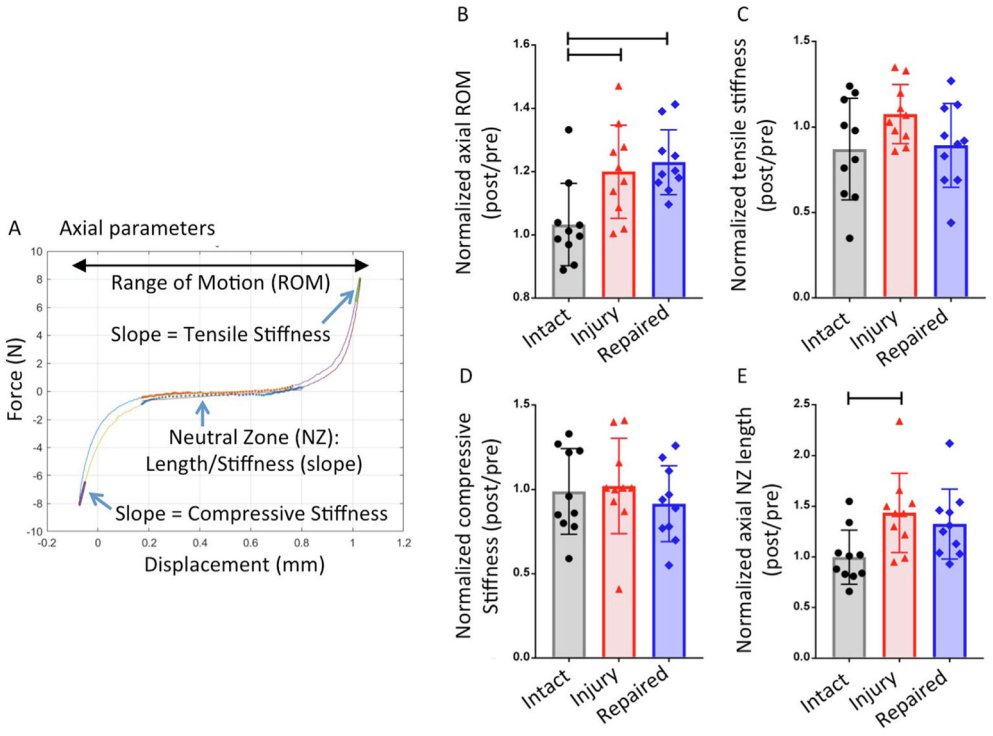

Fig. 3.

Axial testing results. (A) Representative force-displacement curve which shows the regions of the curve analyzed to calculate axial parameters. (B) Results of range of motion (ROM) (C) Results of tensile stiffness (D) Results of axial neutral zone (NZ) length. Bar indicates $p < 0.05$.

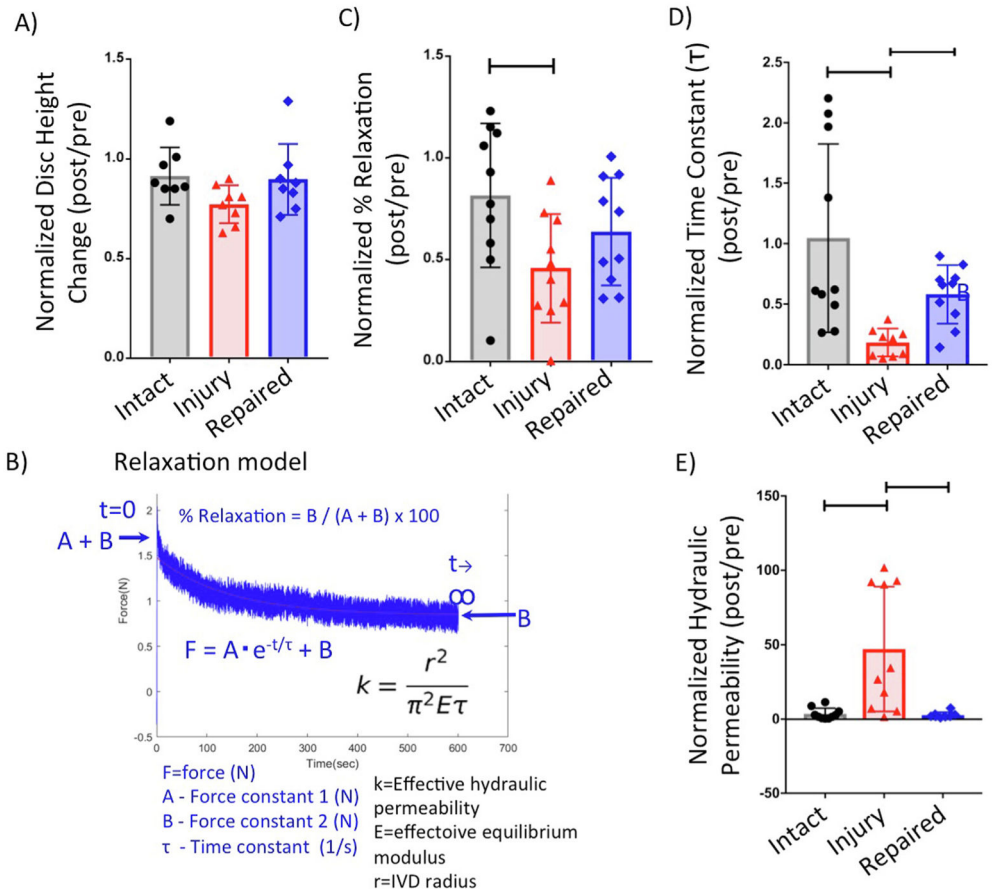

Fig. 4.

Disc height measurement and stress relaxation testing results. (A) Results of disc height ratio. (B) Representative force–time curve of stress relaxation testing and fitted to poroelastic model. Results of (C) %Relaxation, and (D) time constant (τ). (E) Results of effective hydraulic permeability. Bar indicates $p < 0.05$. For stress relaxation testing, the force vs time curve was fitted using a poroelastic model as described (Borde et al., 2015). Relaxation time constant: τ, force constants (A & B); effective equilibrium modulus: (E), intervertebral disc radius: (r), relaxation magnitude: (%Relaxation), and effective hydraulic permeability: (k).

Table 1

Relative changes in all biomechanical parameters and statistical differences for all parameters and conditions (Average ± SD).

Ratio (Post/Pre)	Intact (Average ± SD)	Injured	Repaired	One-way ANOVA P value	Tukey's post-hoc test, P value Intact-Injured	Intact-Repaired	Injured-Repaired
Torque range	0.86 ± 0.27	0.43 ± 0.08	0.40 ± 0.08	*<0.0001	*<0.0001	*<0.0001	0.918
Torsional stiffness	0.84 ± 0.30	0.39 ± 0.10	0.37 ± 0.07	*<0.0001	*<0.0001	*<0.0001	0.946
Torsional neutral zone length	1.00 ± 0.17	1.06 ± 0.25	1.06 ± 0.18	0.742	0.685	0.588	0.986
Axial range of motion	1.00 ± 0.13	1.20 ± 0.15	1.23 ± 0.10	*0.0039	*0.0186	*0.0052	0.861
Tensile stiffness	0.87 ± 0.28	1.08 ± 0.17	0.89 ± 0.24	0.138	0.168	0.931	0.303
Compressive stiffness	0.99 ± 0.30	1.02 ± 0.28	0.92 ± 0.27	0.645	0.948	0.436	0.623
Axial neutral zone length	1.00 ± 0.27	1.43 ± 0.39	1.33 ± 0.35	*0.0206	*0.0414	0.165	0.771
Disc height	0.91 ± 0.14	0.77 ± 0.01	0.90 ± 0.18	0.123	0.145	0.972	0.214
% Relaxation	0.82 ± 0.36	0.46 ± 0.27	0.64 ± 0.27	*0.0411	*0.0319	0.390	0.380
Time constant (τ)	1.45 ± 0.87	4.02 ± 2.04	1.70 ± 0.31	*0.0001	*0.0008	0.917	*0.0023
Effective hydraulic permeability	3.61 ± 3.78	47.130 ± 2.00	2.78 ± 2.00	*0.0011	*0.002	0.930	*0.0049

*: $p < 0.05$.

Table 2

Values for biomechanical parameters (Average ± SD).

		Intact			Injured			Repaired		
	Unit	**Test1**	**Test2**	***p* value**	**Test1**	**Test2**	***p* value**	**Test1**	**Test2**	***p* value**
Torque range	Nm	0.081 ± 0.022	0.073 ± 0.036	0.196	0.090 ± 0.016	0.038 ± 0.009	*<0.01	0.093 ± 0.016	0.037 ± 0.011	*<0.01
Torsional stiffness	Nm/rad	0.457 ± 0.113	0.402 ±0.191	0.126	0.490 ± 0.090	0.191 ± 0.047	*<0.01	0.489 ± 0.077	0.182 ± 0.057	*<0.01
Torsional Neutral Zone length	rad	0.111 ± 0.022	0.108 ± 0.014	0.702	0.104 ± 0.021	0.107 ± 0.016	0.733	0.102 ± 0.016	0.106 ± 0.010	0.593
Axial Range of motion	mm	0.937 ± 0.137	0.971 ± 0.203	0.193	0.944 ± 0.144	1.123 ± 0.160	*<0.01	0.950 ± 0.140	1.171 ± 0.213	*<0.01
Tensile stiffness	N/mm	70.563 ± 23.071	60.528 ± 28.204	0.231	66.946 ± 16.353	72.137 ± 19.530	0.144	65.914 ± 14.131	59.769 ± 23.763	0.258
Compressive stiffness	N/mm	93.154 ± 30.822	90.415 ± 36.244	0.744	96.050 ± 34.224	90.826 ± 17.569	0.668	94.664 ± 34.852	83.245 ± 25.425	0.127
Axial Neutral Zone length	mm	0.469 ± 0.197	0.452 ± 0.185	0.655	0.486 ± 0.204	0.655 ± 0.189	*<0.01	0.478 ± 0.189	0.623 ± 0.247	*<0.01
Disc height	No units	0.305 ± 0.029	0.276 ± 0.032	0.106	0.326 ± 0.025	0.251 ± 0.034	*<0.01	0.308 ± 0.039	0.271 ± 0.023	0.07
% Relaxation	No units	33.493 ± 6.562	27.376 ± 11.297	0.102	34.277 ± 8.120	14.759 ± 8.028	*<0.01	33.802 ± 6.083	20.364 ± 5.976	*<0.01
Time constant (τ)	sec	138.813 ± 58.342	135.867 ± 112.880	0.935	149.399 ± 74.872	34.759 ± 33.987	*<0.01	155.288 ± 57.990	82.943 ± 40.324	*<0.01
Effective hydraulic permeability	10^{-14}m^4/(N*sec)	9.166 ± 5.030	0.327 ± 0.457	0.126	0.106 ± 0.000	0.038 ± 0.038	*<0.012	9.121 ± 7.944	0.427 ± 0.567	0.099

p value: *t*-test.

*: $p < 0.05$.